Available online at www.worldnewsnaturalsciences.com

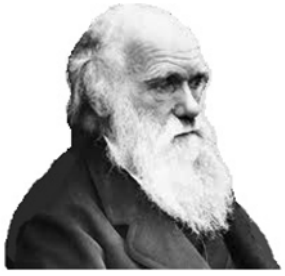

World News of Natural Sciences

WNOFNS 14 (2017) 11-35 EISSN 2543-5426

Packed-Bed Column Adsorption of Metanil Yellow (MY) from Simulated Wastewater using Granular NaOH-Activated Carbon from Cassava (*Manihot esculenta*) Peels

B. O. Isiuku[1,*], M. Horsfall Jr.[2]

[1]Department of Chemistry, Imo State University, P.M.B. 2000, Owerri, Nigeria

[2]Department of Pure and Industrial Chemistry, University of Port Harcourt, P. M. B. 5323 Choba, Port Harcourt, Nigeria

[1,2]E-mail address: obinnabisiuku@yahoo.com horsfalljnr@yahoo.com

*Corresponding author: Tel. +2348035733100, obinnabisiuku@yahoo.com

ABSTRACT

The ability of NaOH-activated carbon derived from cassava peels waste to remove MY from aqueous solution was carried out in a fixed-bed column adsorber. The parameters studied included initial solution concentration, C_o, carbon bed height and volume flow rate. The temperature of operation and initial solution pH were 29 °C and 5.32, respectively. The optimum adsorption capacity, q_e 4.12 mg/g was obtained at C_o 10mg/L, bed height 10cm and flow rate, 13.3ml/min. Experimental data were analyzed with Langmuir, Freundlich and Temkin isotherm, as well as the Thomas, Yoon-Nelson and Clark kinetic models. All the models were good fits for experimental data based on correlation coefficient, R^2 values. The ΔG_{ads} and Freundlich n (1.587) show that the biosorption was spontaneous, good and physical. Results show that NaOH-activated carbon from cassava peels has low capacity to remove MY from aqueous solutions.

***Keywords*:** Adsorption, cassava peels, fixed-bed, metanil yellow, modeling

1. INTRODUCTION

Urbanization and industrialization contribute to a large extent in environmental pollution. In many parts of the world especially in developing countries, polluted water is discharged into streams, wells, rivers and other water bodies without proper treatment (Nwabanne and Igbokwe). Pollution from wastewater depreciates land values, increases municipal costs and causes numerous harmful biological and health effects (Ong et al., 2007). Azo dyes are widely used in textile dyeing, paper printing and other industrial processes such as manufacture of pharmaceutical drugs, toys and foods. Dyes characterized by the presence of at least one azo linkage (-N=N-) bearing aromatic rings, dominates the worldwide market of dyestuffs with a share of about 70% (Ahmad and Hameed, 2010; Osma et al., 2007; Soares et al., 2002).

MY is an azo, water-soluble dye. Although it is a non-permitted colour, it is still widely used as a colorant in sweet meat, ice creams, soft drinks and beverages. Due to its orange yellow colour, MY is extensively used for coating turmeric. It is widely used in colouring leather, paper and in textile industries and also as a stain and colorant for wool. It is used in colouring lacquers and cosmetic products. The dye is suitable for preparing water-fast inks (Mittal et al., 2008; Zimmerman, 1933). Toxicity data reveals that oral feeding of intraperitoneal and intratesticular administration of MY in animals produces testicular lesions due to which seminiferous tubules suffer damage and rate of spermatogenesis is decreased. On oral consumption, it causes toxic methaemoglobinaemia (Sachdeva et al., 1992) cyanosis (Chandro and Nagaraja, 1987) in humans, while skin contact results into allergic dermatitis (Hausen, 1994). MY creates intestinal (Ramchandani et al., 1997) and enzymic (Das et al., 1997) disorders in the human body. It is not mutagenic but can alter the expression genes (Gupta et al., 2003).

Removal of toxic industrial, water-soluble non-biodegradable wastes, particularly organic dyes is of great concern. Hence, removal of coloured wastes from wastewater is of significant importance. Physicochemical oxidation, froth floatation, etc., have been used for the removal of organics as well as inorganics from wastewater (Mittal et al., 2008). Using sophisticated instruments, electrochemical processes like electrochemical degradation (Fan et al., 2006), electro-coagulation (Daneshvar et al., 2006), electrochemical oxidation (Rajkumar and Kim, 2006) and photoelectrocatalytic methods (Ahmad and Hameed, 2010; Gupta et al., 2007), the task to eradicate toxic pollutants from water have been accomplished. Adsorption is considered one of the most efficient due to its easy methodology and operations. Activated carbon (AC) is a widely used adsorbent in the treatment of wastewater because it possesses desirable physicochemical properties including good mechanical strength, chemical stability in diverse media, and large pore size distribution in addition to its extensive specific surface area (Zhu and Yuan, 2011). Because commercial ACs are expensive, emphasis is currently placed on the preparation of low-cost ACs from agricultural by-products, which are from renewable sources (Salman et al., 2011; Ren et al., 2011; Li et al., 2010; Petrov et al., 2010; Sun and Webley, 2010; Dolas et al., 2011; Baccar et al., 2010). Investigations have been carried out to remove contaminants from wastewater using fixed-beds. Batch adsorption data are generally not applicable to most treatment systems (such as column operations) where contact time is not sufficient for the attainment of equilibrium. Packed - bed column operation is preferred to the batch operation for the removal of micro-pollutants when dealing with large volumes of wastewater (Banat et al., 2007).

The aim of this work was to produce activated carbon from cassava peels and explore its efficacy in the removal of MY in a fixed-bed column. The effects of C_o, carbon bed height and dye solution volume flow rate were studied.

2. MATERIALS AND METHODS

The MY (Merck) used in this work, was purchased at Onitsha, Nigeria and used with no further treatment. Fig. 1 shows the structure. Stock solution was prepared by dissolving 1g per litre solution using distilled water.

2. 1. Preparation of activated carbon

The method of Pokordi and Vasanth Kumar, (2006) was used. The cassava peels used in this work was obtained from Egbeada in the Mbaitoli Local Government Area of Imo State, Nigeria. The biomass was washed to remove dirt and soil, and dried in a hot-air oven. The dry biomass was carbonized at 500 °C for 7h and cooled. The char was ground and sieved to get 0.595 – 1.68 mm size particles, which were impregnated with 4.17% $^{w}/_{v}$ NaOH solution at a ratio of 1 char: 3 alkali w/w. Excess alkali was drained off after 24h. The carbon was dried and heated at 500 °C for 4h. After cooling, the carbon was leached with hot distilled water to pH ≈6. The carbon was dried in a hot-air oven at 110 °C for 2h. It was cooled and packaged in an airtight plastic container. The AC was analyzed for physicochemical properties.

2. 2. Fixed-bed adsorption process

The fixed-bed column was made of Pyrex glass cylinder 1cm inner diameter and 43cm length. The method of Ahmad and Hameed, (2010) was used. The bottom of the column was plugged with glass wool. A known mass of AC equivalent to 10, 20 or 30 cm height was packed in the column and the carbon sealed with glass wool. Glass beads were introduced to occupy the space above the carbon. This enhanced uniform flow of the adsorbate. Dye solution of C_o (10, 50 or 100 mg/L) at pH 5.32 was pumped upward with a metering pump (Chem-Tech Pal No. 0-111.808) at a known flow rate (13.3, 25 or 34 ml/min), and temperature 29 °C. Effluent samples were collected at regular intervals of 30min and analyzed with a UV/Vis spectrophotometer (Shimadzu UV-752, Japan) at λ_{max} 440nm. Different C_o were got by diluting the stock solution with distilled water.

2. 3. Characterization of activated carbon

The bulk and dry densities, and porosity were determined by the method of Ekpete et al., (2012); pore volume by the method of Mohammed et al., (2012); specific surface area by the ethylene glycol monoethyl ether (EGME) method (Cerator and Luteneger, 2002); Iodine number by the method of Gimba and Musa, (2005); pH by the ASTM D 3838 – 80 standard test method, (1996); moisture, volatile matter, ash, and fixed carbon contents by the methods of Rengaraj et al., (2002); AOAC, 1990; Isiuku et al., (2015) respectively.

2. 4. Fixed-bed column adsorption analysis

The time for breakthrough appearance and the shape of the breakthrough curve are paramount in determining the operation and the dynamic response of an adsorption packed – bed column. The breakthrough curves show the loading behaviour of the dye to be removed from solution in a packed-bed column and is usually expressed in terms of adsorbed dye concentration C_{ad}, or normalized concentration C_t/C_o, as a function of time or volume of effluent for a given bed height (Ahmad and Hameed, 2010; Isiuku et al., 2014; Aksu and Gönen, 2004; Taty-Custodes et al., 2005). Effluent volume $V_{eff.}$, can be calculated from Eq. 1:

$$V_{eff} = Qt_{tot} \quad \text{..... (1)}$$

where: t_{tot} (min) is the total flow time. The area under the breakthrough curve A, obtained by integrating the adsorbed concentration C_{ad} (mg/L) against time (min) plot can be used to find the total adsorbed dye quantity q_{tot} (mg). q_{tot}, for a given C_o and flow rate is calculated from Eq. 2:

$$q_{tot} = \frac{QA}{1000} = \frac{Q}{1000}\int_{t_o}^{t_{tot}} C_{ad}\, dt \quad \text{... ... ... (2)}$$

Total amount of dye sent to the column m_{tot} is determined from Eq. 3:

$$m_{tot} = \frac{C_e Q t_{tot}}{1000} \quad \text{... ... ... (3)}$$

Total removal R (%) of dye (column performance) with respect to flow volume can be determined from the ratio of q_{tot} to m_{tot}, Eq. 4:

$$R(\%) = \frac{100 q_{tot}}{m_{tot}} \quad \text{... ... ... (4)}$$

Equilibrium uptake of the dye in the column per unit mass of dry adsorbent x (g), q_e (mg/g) is defined by Eq. 5 as:

$$q_e = \frac{q_{tot}}{x} \quad \text{... ... ... (5)}$$

Un-adsorbed dye concentration at equilibrium in the column C_e (mg/L) is given by Eq. 6:

$$C_e = \frac{(m_{tot} - q_{tot})1000}{V_{eff}} \quad \text{... ... ... (6)}$$

$$C_e = \frac{(m_{tot} - q_{tot})1000}{Qt_{tot}} \quad \text{... ... ... (7)}$$

2. 4. 1. Isotherm modelling

Adsorption isotherms portray the distribution of adsorbate particles between the liquid phase and the solid phase as the adsorption reaches equilibrium (Bello et al., 2012). In this work, experimental results were analyzed with the Langmuir, Freundlich and Temkin isotherm models.

2. 4. 1. 1. Langmuir isotherm model

The Langmuir isotherm is based on the assumption that a fixed number of adsorption sites are available, and the adsorption is reversible. The model also assumes that the surface of the adsorbent is homogenous (Nidheesh et al., 2012). The model equation is expressed as Eq. 8:

$$q_e = \frac{q_m K_L C_e}{1 + K_L C_e} \quad \ldots\ldots\ldots\ldots\ldots\ldots\ldots\ldots\ldots \quad (8)$$

The linear form of Eq.8 is expressed as Eq.9:

$$\frac{1}{q_e} = \frac{1}{q_m} + \left(\frac{1}{q_m K_L}\right)\frac{1}{C_e} \quad \ldots\ldots\ldots\ldots\ldots\ldots\ldots\ldots \quad (9)$$

where: K_L (L/g) is a constant that increases with increasing particle size, q_m (mg/g) is the amount of adsorbate adsorbed to form a complete monolayer on the adsorbent surface. A plot of $1/q_e$ vs $1/C_e$ gives a straight line with slope and intercept equal to $1/q_m K_L$ and $1/q_m$ respectively.

The favourability of the biosorption process was confirmed (Bello et al., 2012) by applying the separation factor R_L expressed as Eq. 10:

$$R_L = \frac{1}{1 + K_L C_{om}} \quad \ldots\ldots\ldots\ldots\ldots\ldots\ldots\ldots\ldots\ldots \quad (10)$$

where: C_{om} is the maximum influent concentration.

2. 4. 1. 2. Freundlich isotherm model

The Freundlich isotherm is based on non-ideal biosorption that involves heterogeneous surface energy systems. It is expressed (Dutta et al., 2012) in the logarithmic form as Eq. 11:

$$Inq_e = InK_F + \frac{1}{n} InC_e \quad \ldots\ldots\ldots\ldots\ldots\ldots\ldots \quad (11)$$

where: K_F is the Freundlich constant which is a rough indicator of the biosorption capacity and 1/n is the biosorption intensity. A plot of In q_e vs In C_e gives a straight line with slope equal to 1/n and intercept equal to In K_F.

2. 4. 1. 3. Temkin isotherm model

The Temkin model describes the heat of biosorption and interaction between biosorbate and biosorbent particles (Dutta et al., 2012). It is expressed as Eq. 12:

$$q_e = \frac{RT}{b_T} In\, A_T + \frac{RT}{b_T} In\, C_e \quad \ldots\ldots\ldots\ldots\ldots\ldots \quad (12)$$

where: A_T and b_T are Temkin constants. Plots of q_e vs In C_e gives a straight line, with slope equal to RT/bT, and intercepts equal (RT/b_T) In A_T.

2. 4. 2. Column adsorption modelling

To design a column adsorption process, it is vital to predict the breakthrough curve and adsorption capacity of the adsorbent for the selected adsorbate under the given set of operating conditions. It is also important for determining maximum column adsorption capacity which is important to any adsorption system (Isiuku et al., 2014; Patel and Vashi, 2012).

Mathematical models have been developed for the determination of efficiency and applicability of the column models for large scale operations. They include the Thomas and Yoon-Nelson models which were applied in this study.

2. 4. 2. 1. The Thomas model

The Thomas model (Nidheesh et al., 2012) is one of the most commonly used models in fixed-bed column adsorption process. It is expressed as Eq. 13:

$$\frac{C_t}{C_o} = \frac{1}{1 + exp\left[K_{Th}\left(q_o 1000x - C_o V_{eff}\right)/Q\right]} \ldots\ldots\ldots\ldots\ldots\ldots\ldots (13)$$

where: C_t (mg/L) is the effluent dye concentration at time, t (min), K_{Th} (ml/mg/min) is the Thomas rate constant and q_o (mg/g) is the estimated adsorption capacity of the adsorbent.

The value V_{eff} can be obtained by the expression Eq. 14:

$$V_{eff} = Qt_{tot} \ldots\ldots\ldots\ldots\ldots\ldots\ldots\ldots\ldots\ldots\ldots\ldots\ldots\ldots\ldots\ldots (14)$$

The linearized form of the Thomas equation is expressed as Eq.15:

$$In\left[\left({}^{C_o}/_{C_t}\right) - 1\right] = \frac{K_{Th} q_o 1000x}{Q} - K_{Th} C_o t \ldots\ldots\ldots\ldots\ldots (15)$$

Figs 5-7 show plots of ln [(C_o/C_t) – 1] against t that are straight lines for various C_o (at fixed bed height and flow rate), bed height (at fixed C_o and flow rate) and flow rate (at fixed C_o and bed height). Table 2 shows the Thomas parameters at various conditions. The values show that as q_o, increased, the rate constant decreased. Also, q_o increased with increase in C_o, increase in bed height and decrease in flow rate. The result agrees with literature (Ahmad and Hameed, 2010). The R^2 values show that Thomas model fitted experimental data well.

2. 4. 2. 2. The Yoon-Nelson model

The linearized form of the Yoon-Nelson model (Salman et al., 2011) is expressed as Eq. 16:

$$In\left[\frac{C_t}{(C_o - C_t)}\right] = K_{YN} - \tau K_{YN} \ldots\ldots\ldots\ldots\ldots\ldots\ldots\ldots\ldots (16)$$

where: K_{YN} (L/min) is the Yoon-Nelson constant, τ (min) is the time required for 50% adsorbate breakthrough, and t (min) is the sampling time.

Figs 8-11 show plots of $\ln[C_t/(C_o-C_t)]$ against t for different C_o (at fixed bed height and flow rate), bed heights (at fixed C_o and flow rate) and flow rate (at fixed C_o and bed height). Straight lines were obtained from which K_{YN} values were determined from the intercepts and τ values from the slopes (Table 4). The q_o from the Yoon-Nelson model (Patel and Vashi, 2012; Sivakumar and Palanisamy, 2009b) was determined from Eq. 17:

$$q_o = \frac{q_{tot}}{x} = \frac{C_o Q \tau}{1000x} \ldots\ldots\ldots\ldots\ldots\ldots\ldots\ldots\ldots (17)$$

The R^2 values show that the Yoon-Nelson model simulated experimental data well. Table 4 also shows increase in q_o with increase in τ, increase in bed height and decrease in flow rate. q_o increased with decrease in K_{YN}. These results have the same trend with literature (Ahmad and Hameed, 2010).

2. 4. 2. 3. Clark Kinetic model

The Clark kinetic model uses the Freundlich model constant n to give a procedure for simulating breakthrough curves. The linearized form (Dutta et al., 2012) of the Clark model is expressed as Eq. 18:

$$In\left[\left(\left(\frac{C_o}{C_t}\right)^{n-1} - 1\right]\right. = In\, A - rt \quad \ldots\ldots\ldots\ldots\ldots\ldots\ldots (18)$$

where: A and r (min^{-1}) are Clark constants. A plot of $In\left[\left(\left(\frac{C_o}{C_t}\right)^{n-1} - 1\right]\right.$ vs t gives a straight line with slope equal to r and intercept equal to In A.

3. RESULTS AND DISCUSSION

3. 1. Effect of initial solution concentration

The effect of C_o on the breakthrough curves at bed height 20cm, flow rate 13.3ml/min and pH 5.32 is shown in Fig.2. It is observed that for all the C_o values used, before the first 30min, the adsorption had reached over 90% of the C_o which is near saturation point (Han et al., 2007). However, the q_e 0.53, 0.73 and 2.82mg/g for C_o values 10, 50 and 100mg/L respectively show that the q_e (mg/g) increased with increase in C_o. This result is in agreement with literature (Salman et al., 2011).

The increase in q_e with increase in C_o can be explained by the fact that more adsorption sites were being covered as the C_o increased (Engin, 2009). Experimental data (Table 2) show 100mg/L as the optimum C_o.

3. 2. Effect of carbon bed height

The effect of carbon bed height on the adsorption of MY on NaOH-activated carbon from cassava peels at C_o 10 mg/L, pH 5.32 and Q 13.3 ml/min is depicted in Fig. 3. The figures show a breakthrough curve with breakthrough time of 120min and exhaustion time of 360 min for bed height 10 cm.

The q_e values 4.12, 0.53 and 0.21 mg/g for bed heights 10, 20 and 30 cm respectively show that q_e increased with decrease in bed height. This result agrees with literature. This shows that at smaller bed height the effluent adsorbate concentration ratio increased more rapidly than for a higher bed height. Furthermore, the bed is saturated in less time for smaller bed heights. Small bed height corresponds to fewer amounts of adsorbent Nwabanne and Igbokwe, 2012).

3. 3. Effect of flow rate

The effect of flow rate on the adsorption of MY on NaOH-activated carbon from cassava peels at C_o 10 mg/L, bed height 20 cm, and pH 5.32 is shown in Fig. 4. The figure shows a breakthrough curve with breakthrough point at 60 min and saturation point at 330 min. The figure also shows that at higher flow rate, saturation was faster. The q_e values 0.634, 0.518 and 0.428 mg/g for flow rate, 13.3, 25 and 34 ml/min respectively show that q_e increased with decrease in flow rate.

This agrees with the literature (Nidheesh et al., 2012). This is attributed to the fact that as the contact time between the adsorbate and the adsorbent decreased the adsorption efficiency in the carbon bed reduced. At higher flow rate, the movement of adsorption zone along the bed was faster decreasing the time for adsorption of the MY on the carbon bed (Al-Fatlawi and Neamah, 2015).

3. 4. Isotherm modelling

3. 4. 1. Langmuir isotherm model

A plot of $1/q_e$ vs $1/C_e$ gave a straight line (Fig. 5) from which the slope and intercept, K_L and q_m were determined. The values of K_L and q_m are shown in Table 3. The R^2 (0.6575) value shows that Langmuir model is a good fit for modelling the adsorption process.

The favourability of the biosorption was confirmed (Bello et al., 2012) by applying the Hall separation factor R_L, expressed as Eq. 10. The R_L value (0.172) shows that the process was favourable since $R_L < 1$.

3. 4. 2. Freundlich isotherm model

Fig. 6 shows a plot of In q_e vs In C_e. The values of K_F, 1/n and n are shown in Table 3. The value of n (1.587), shows that the adsorption was a good, favourable and physisorption process (Al-Fatlawi and Neamah, 2015). The R^2 value (0.7116) shows the Freundlich model is a good fit for analyzing experimental data.

3. 4. 3. Temkin isotherm model

A plot of q_e vs In C_e gave a straight line (Fig. 7). Table 3 shows the values of A_T and b_T. The R^2 value (0.6111) shows that the Temkin isotherm is a good fit for analyzing experimental data.

3. 5. Kinetic modelling

3. 5. 1. Application of the Thomas model

Experimental adsorption data were analysed with the Thomas model in order to determine the Thomas parameters shown in Figs. 8-10 and Table 4, for various C_o, bed heights and flow rates. The figures and table show that at constant bed height and flow rate, q_o increased with increase in C_o while K_{TH}, decreased. The R^2 values which are above 0.9 shows that this model is a good fit. All results show that the Thomas model analysed the experimental data well at all C_o, bed height and flow rate. The results are in agreement with literature (Nwabanne and Igbokwe, 2012; Baek et al., 2007).

3. 5. 2. Application of Yoon-Nelson kinetic model

Experimental data were analysed with the Yoon-Nelson kinetic model to determine the model parameters K_{YN}, τ, q_o and R^2 values at various C_o, bed heights and flow rates, pH 3 and temperature 29 °C. The plots are shown in Figs. 11-13, and values of parameters in Table 5. Results show that K_{YN} and q_o increased with increase in C_o; q_o and τ increased with increase in bed height but the τ decreased; q_o and τ values decreased with increase in flow rate. The values of R^2 in all the conditions were generally above 0.9 showing that the Yoon-Nelson model simulated experimental data well.

3. 5. 3. Application of Clark kinetic model

A plot of $In\left[\left(\left(\frac{C_o}{C_t}\right)^{n-1} - 1\right]\right.$ vs t gave a straight line (Fig. 14-16). The values of A, n and r are shown in Table 6. The R^2 (> 0.95) shows that Clark model simulated experimental data well.

3. 6. Spontaneity of the biosorption process

The spontaneity of the process was determined (Depci et al., 2012) by applying Eq. 19:

$$\Delta G^o_{ads} = RTInK_D \quad \ldots\ldots\ldots\ldots\ldots\ldots \quad (19)$$

where: ΔG^o_{ads} is the standard free energy of biosorption, R (8.314 J/mol/K) is the gas constant, T (K) is the absolute temperature and K_D is the equilibrium distribution constant. K_D is determined (Salman et al., 2011) from Eq. 20:

$$K_D = \frac{(C_o - C_e)e}{C_e} \quad \ldots\ldots\ldots\ldots\ldots\ldots \quad (20)$$

The K_D values for C_o 10, 50 and 100 mg/L were determined as 0.034, 0.009 and 0.017 respectively. The ΔG^o_{ads} values were calculated to be -8.49, -11.827 and -10.23 kJ/mol for C_o 10, 50 and 100 mg/L respectively. The magnitudes of these values and their negative values show that the process was spontaneous for all C_o values. The Freundlich constant n value (1.587) shows that the adsorption was good and physical (Al-Fatlawi and Neamah, 2015).

4. CONCLUSION

Sodium hydroxide-activated carbon prepared from cassava peels waste was used to remove MY from aqueous solution in a fixed-bed column. Effects of C_o, bed height and flow rate were studied after adsorption times of 480 min for various C_o and bed heights, and 360 min for flow rate. q_e increased with increase in C_o and decrease in flow rate. However, q_e increased with decrease in carbon bed height. The highest q_e of 4.12 mg/g was obtained with C_o 10 mg/L, bed height 10 cm and bed height 13.3 ml/min. Langmuir, Freundlich and Temkin isotherm, as well as Thomas, Yoon-Nelson and Clark kinetic models simulated experimental data well as shown by the R^2. The results show very low efficiency in the removal of MY from aqueous solution by NaOH-activated carbon from cassava peels.

References

[1] Nwabanne, J. I. & Igbokwe, P. K. (2012). Adsorption performance of packed-bed column for the removal of lead(II) using oil palm fibre, *Inter. J. Appl. Technol*. 2(5), 106-115

[2] Ong, S., Seng, C. & Lim, P. (2007). Kinetics of adsorption of Cu(II) and Cd(II) from aqueous solution on husk and modified rice husk, *EJEFChe*. 6(2), 1764-1774

[3] Ahmad, A. A. & Hameed, B. H. (2010). Fixed-bed adsorption of reactive azo dye onto granular activated carbon prepared from waste, *J. Hazard. Mater*. 17, 298-303

[4] Osma, J. F., Saravia, V., Toca-Herrera, J. I., Couto, S. R. (2007) .Sunflower seed shells: a novel and effective low-cost adsorbent for the removal of the diazo dye Reactive Black 5 from aqueous solutions, *J. Hazard. Mater*. 147, 900-905

[5] Soares, G. M. B., Amorim, M. T. P., Hrdina, R. & Costa-Ferreira, M. (2002). Studies on the biotransformation of novel diazo dyes by laccas, *Process Biochem*. 37, 582-587

[6] Mittal, A., Gupta, V. K., Malviya, A & Mittal, J. (2008.) Process development for the batch and bulk removal and recovery of a hazardous, water-soluble azo dye (metanil yellow) by adsorption over waste materials (bottom ash and de-oiled soya), *J. Hazard. Mater*. 151, 821-832

[7] Zimmerman, E. W. (1933). Coloured water - proof drawing inks, *Ind. Eng. Chem.* 25, 1033

[8] Sachdeva, S. M., Mani, K. V. Adval, S. K., Jalpota, V. P., Rasela, K. C. & Chadha, D. S. (1992). Acquired toxic methaemoglobinaemia, *J. Assoc. Physicians Ind.* 40, 239-240

[9] Chandro, S. S. & Nagaraja, T. (1987). A food-poisoning out-break with chemical dye: an investigation report, *Med. J. Armed Forces Ind.* 43, 291-300

[10] Hausen, B. M. (1994). A case of allergic contact dermatitis due to metanil yellow, *Contact Dermatitis* 31, 117-118

[11] Ramchandani, S. M., Das, M., Joshi, A. & Khanna, S. K. (1997). Effect of oral and parental administration of metanil yellow on some hepatic and intestinal biochemical parameters, *J. Appl. Toxicol*. 17, 85-91

[12] Das, M., Ramchandani, S., Upreti, R. K. & Khanna, S. K. (1997). Metanil yellow: a bifunctional inducer of hepatic phase I and phase II xenoblastic-metabolizing enzymes, *Food Chem. Toxicol*. 35, 835-838

[13] Gupta, S., Sundarrajan, M. & Rao, K. V. K. (2003). Tumor promotion by metanil yellow and malachite green during rat hepatocarcingenesis associated with dysregulated expression of cell cycle regulatory proteins, *Tertogen. Carcin. Mut*. (Suppl. I), 301-312

[14] Fan, L., Zou, Y., Yang, W., Chern, G. & Yan, F. (2006). Electro-chemical degradation of amaranth aqueous solution on ACF, *J. Hazard. Mater*. 137, 1182-1188

[15] Daneshvar, N., Oladegaragoze, A. & Djafarzadeh, N. (2006). Decolourization of basic dye solutions by electro-coagulation: an investigation of the effect of operational parameters, *J. Hazard. Mater*. 129, 116-122

[16] Rajkumar, D. & Kim, J. G. (2006). Oxidation of various reactive dyes with in-situ electro-generated active chlorine for textile dyeing: Industrial wastewater treatment, *J. Hazard. Mater*. 13, 203-212

[17] Gupta, V. K., Mittal, A., Jain, R., Mathur, M. & Sikarwar, S. (2007). Photochemical degradation of hazardous dye-safranine –T using TiO_2 catalyst, *J. Colloid Interf. Sci*. 309, 464-469

[18] Zhu, H., Yang, X., Mao, Y., Cheng, Y., Long, X. & Yuan, W. (2011). Adsorption of EDTA on activated carbon from aqueous solutions, *J. Hazard. Mater*. 185, 195-957

[19] Salman, J. M., Njoku, V. O. & Hameed, B. H. (2011). Batch and fixed-bed adsorption of 2,4-dichlorophenoxyacetic acid onto oil palm frond activated carbon, *Chem. Eng. J*. 174, 33-40

[20] Ren, L., Zhang, J., Li, Y. & Zhang, C. (2011). Preparation and evaluation of cattail fibre-based activated carbon for 2,4-dichlorophenol and 2,4,6-trichlorophenol removal, *Chem. Eng. J*., 168, 553-561

[21] Li, W., Zhang, J., Wang, Y. & Li, Y. (2010). Adsorptive removal of Cr(VI) by Fe-modified activated carbon prepared from *Trapa natans* husk, *Chem. Eng. J*. 162, 677-684

[22] Petrov, B., Budinova, T., Tsyntsarski, B., Kachkodan, V., Shkavro, Z. & Petrov, N. (2010). Removal of aromatic hydrocarbons from water by activated carbon from apricot stones, *Chem. Eng. J*. 165, 258-264

[23] Sun, Y. & Webley, P. A. (2010). Preparation of activated carbon from corn cob with large specific surface area by a variety of chemical activators and their application in gas storage, *Chem. Eng. J*. 162, 883-892

[24] Dolas, H., Sahin, O., Saka, C. & Demir, H. (2011). A new method in producing high surface area activated carbon: the effect of salt on the surface area and the pore size distribution of activated carbon prepared from pistachio shell, *Chem. Eng. J*. 166, 191-197

[25] Baccar, R., Blanquez, P., Bouzid, J., Feki, M. and Sarra, M. (2010). Equilibrium, thermodynamic and kinetic studies on adsorption of commercial dye by activated carbon derived from olive-waste cakes, *Chem. Eng. J*. 165, 457-464

[26] Banat, F., Al-Sheh, S., Al-Ahmad, R. & Bni-Khalid, F. (2007). Bench-scale and packed-bed sorption of methylene blue using treated olive pomace and charcoal, *Bioresour. Technol*. 98(16), 3017-3025

[27] Pokordi, K. & Vasanth Kumar, K. (2007). Equilibrium, Kinetics and Mechanism modelling and simulation of basic and acid dyes sorption onto jute fibre carbon: Eosin yellow, malachite green and crystal violet single component systems, *J. Hazard. Mater*. 143(1-2), 311-327. doi:10.1016/j.jhazmat.2006.09.029

[28] Ekpete, O. A. (2012). Adsorption and kinetic studies of phenol and 2-chlorophenol onto fluted pumpkin (*Telfairia occidentalis*, Hook) stem waste activated carbon *PhD Dissertation*, University of PortHarcourt, PortHarcourt, Nigeria

[29] Mohammed, A., Aboje, A. A., Auta, M. & Jibril, M. (2012) .A comparative analysis and characterization of animal bones as adsorbent, *Adv. Appl. Sci. Res.* 3(5), 3089-3096

[30] Cerator, A. B. & Luteneger, A. J. (2002). Determination of surface area of fine grained soils by the ethylene glycol monoethly ether (EGME) method, *J. Geotech. Testing* 25(3), 1-7

[31] Gimba, C. & Musa, I. (2005). Adsorption of phenols and some toxic metals from textile effluents, In Proceedings of the 28th Annual International Conference of Chemical Society of Nigeria, 32, 167-170

[32] American Standard Test Method for Testing and Materials, (1996). Annual Book of ASTM Standard, Vol. 15.01 Refractories, Carbon and Graphic Products; Activated Carbon, ASTM, Philadelphia PA

[33] Rengaraj, S., Seung-Hyeon, M. & Sivabam, S. (2002). Agricultural solid waste for the removal of organics: Adsorption of phenol from water and waste water by palm seed coat activated carbon, *Waste Manage*. 22, 543-548

[34] Association of Official Analytical Chemists (AOAC) (1990). *Official Methods of Analysis* 15th Ed. Arlington, VA

[35] Isiuku, B. O. (2015). Adsorption of metanil yellow and methyl red from aqueous solutions using cassava peels activated carbon in a fixed-bed column, PhD Dissertation, University of Port Harcourt, Port Harcourt, Nigeria

[36] Isiuku, B. O., M. Horsfall Jnr., M. & A.I. Spiff, A. I. (2014). Colour removal from a simulated methyl red wastewater by adsorption on carbon in a fixed bed, *Res. J. Appl. Sci*. 9(4), 201-207

[37] Aksu, Z. & Gönen, F. (2004). Biosorption of phenol by immobilized activated sludge in a continuous packed bed: prediction of breakthrough curves, *Process Biochem*. 39, 599-613

[38] Taty-Custodes, V. C., Fauduet, H., Porte, C. & Ho, Y. S. (2005). Removal of lead (II) ions from synthetic and real effluents using immobilized *Pinus sylvetris* sawdust: Adsorption on a fixed-bed column, *J. Hazard. Mater*. B123, 135-144

[39] O. S. Bello, O. S., O. M. Adelaide, O. M. M. A. Hameed, M. A. & O. A. M. Popoola, O. A. M. (2010). *Macedonian J. Chem. Chem. Eng*. 29 (1), 77

[40] P. V. Nidheesh, P. V., R. Gandhimathi, R., S. T. Ramesh, S. T. & T. S. A. Singh, T. S. A., *J. Urban Environ. Eng.* 6 (1), 18 (2012)

[41] O. S. Bello, T. A. Fatona, F. S. Falaye, O. M. Osuolale and V. O. Njoku, *Environ. Eng. Sci.* 29 (3), 186 (2012)

[42] M. Dutta, J. K. Basu, M. H. Faraz, N. Gautam, and A. Kumar, *Arch. Appl. Sci. Res.* 4 (2), 882 (2012)

[43] H. Patel and R.T. Vashi, (2012) Fixed-bed column adsorption of Acid Yellow 17 dye onto tamarind seed powder, *Canad. J. Chem. Eng*. 90, 180-185

[44] B.O. Isiuku, M. Horsfall Jnr and A.I. Spiff, (2013). Adsorption of metanil yellow on chemically-activated carbon in a packed-bed column: Effect of activation reagent, *J. Eng. Appl. Sci*. 8(9-12): 282-289

[45] P.Sivakumar and P.N. Palanisamy, (2009b). Adsorptive removal of reactive and direct dyes using non-conventional adsorbent – column studies, *Indian J. Chem. Technol*. 68: 894-899

[46] Y.S. Al-Degs, M.A.M. Kraisheh, J.S. Allen and M.N. Ahmad, (2009). Adsorption characteristics of reactive dyes in columns of activated carbon, *J. Hazard. Mater*. 165: 944-949

[47] R. Han, Y. Wang, W. Yu, W. Zou, J. Shi and H. Liu, (2007). Biosorption of methylene blue from aqueous solution by rice husk in a fixed-bed column, *J. Hazard. Mater*. 141, 713-718

[48] A.B. Engin, (2009). Feasibility analysis of colour removal from textile dyeing wastewater in a fixed-bed column system by surfactant-modified zeolite (SMZ), *J. Hazard. Mater*. 166: 180-185

[49] A. H. Al-Fatlawi, and M. M. Neamah, *Int. J. Adv. Res. Sci. Eng. Technol.* 2 (3), 557 (2015)

[50] K. Baek, S. Song, S. Kang, Y. Rhee, C. Lee, B. Lee, S. Hudson and T. Hwang, (2007). Adsorption kinetics of boron by anion exchange resin in packed column bed. *J. Ind. Eng. Chem.* 13 (3), 452

[51] Depci, T., Kul A. L., Onal, Y., Disli, E., Alkan, S. & Turkmenoglu, Z. F. (2012). *Physicochem. Probl. Miner. Process.* 48 (1), 253

(Received 29 August 2017; accepted 15 September 2017)

Table 1. Physicochemical properties of NaOH-activated carbon from cassava peels

Property	Value
pH	6.83
Specific surface area (m^2/g)	804.2
Pore volume (cm^3/g)	0.04
Porosity	0.86
Bulk density (g/cm^3)	0.19
Dry density (g/cm^3)	0.03
Iodine number (mg/g)	74.82
Moisture content(%)	15.12
Volatile matter content(%)	30.88
Fixed carbon content(%)	45.74
Ash content(%)	8.26

Table 2. Column data parameters obtained at different initial dye concentrations, bed heights and flow rates

Initial Concentration (mg/L)	Carbon bed height (cm)	flow rate (ml/min)	q_{tot} (mg/g)	q_e (mg/g)
10	20	13.3	2.108	0.527
50	20	13.3	2.92	0.73
100	20	13.3	11.28	2.82
10	10	13.3	8.236	4.118
10	30	13.3	1.278	0.213
10	20	25	2.072	0.518
10	20	34	1.712	0.428

Table 3. Thomas kinetic model parameters at different conditions using linear regression analysis.

Initial Conc. (mg/L)	Carbon bed height (cm)	Flow rate (ml/min)	$K_{Th} \times (10^{-4})$ (ml/min.mg)	q_o (mg/g)	R^2
10	20	13.3	1.9	40.57	0.9517
50	20	13.3	0.5	200.4	0.9297
100	20	13.3	0.1	1180.61	0.8019
10	10	13.3	5.2	29.77	0.9443
10	30	13.3	1.6	41.87	0.8824
10	20	25	1.8	99.82	0.9474
10	20	34	3.1	88.13	0.8432

Table 4. Yoon-Nelson kinetic model parameters at different conditions using linear regression analysis

Initial Conc. (mg/L)	Carbon bed height (cm)	flow rate (ml/min)	$K_{YN} \times (10^{-3})$ (min^{-1})	τ (min)	q_o (mg/g)	R^2
10	20	13.3	1.9	1223.16	40.67	0.951
50	20	13.3	2.6	1257.54	209.07	0.9279
100	20	13.3	0.9	3975	1321.69	0.7996
10	10	13.3	5.3	89.74	5.97	0.9432
10	30	13.3	1.7	1787.65	39.63	0.948
10	20	25	4.8	674	42.13	0.9069
10	20	34	2.8	1176	99.69	0.9662

Table 5. Clark kinetic model parameters at different conditions using linear regression analysis.

Initial Conc. (mg/L)	Carbon bed height (cm)	flow rate (ml/min)	r	A	R^2
10	20	13.3	0.0019	17.626	0.9436
50	20	13.3	0.0026	45.568	0.934
100	20	13.3	0.0008	63.288	0.8314
10	10	13.3	0.0013	55.147	0.9564
10	30	13.3	0.0025	44.295	0.596
10	20	25	0.0049	42.415	0.9219
10	20	34	0.0026	45.205	0.9299

Table 6. Isotherm parameter data for fixed-bed biosorption of my on naoh-activated carbon.

Model	Parameter	Value
Langmuir	K_L (L/mg)	0.048
	q_m (mg/g)	63.291
	R_L	0.172
	R^2	0.6575
Freundlich	1/n	0.6303
	n	1.587
	K_F [mg/g(L/mg)]$^{1/n}$	9.305
	R^2	0.7116
Temkin	A_T (L/g)	4.486
	b_T (J/mol)	3014.561
	R^2	0.6111

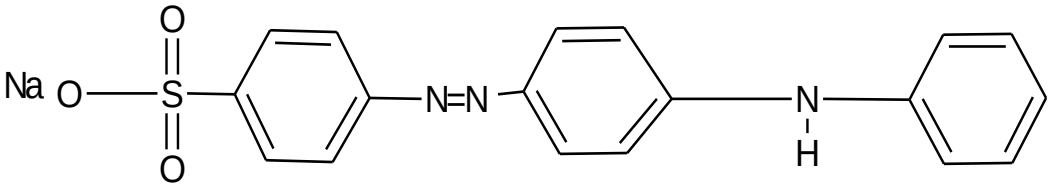

Fig 1. Structure of metanil yellow

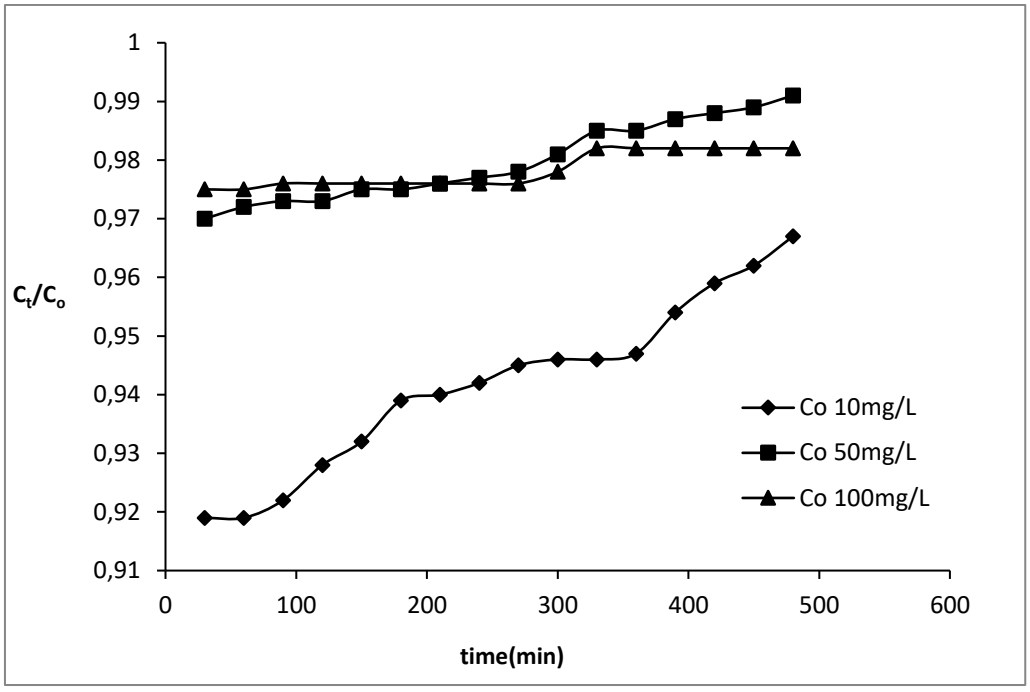

Fig. 2. Adsorption of MY on NaOH- activated carbon at various C_o

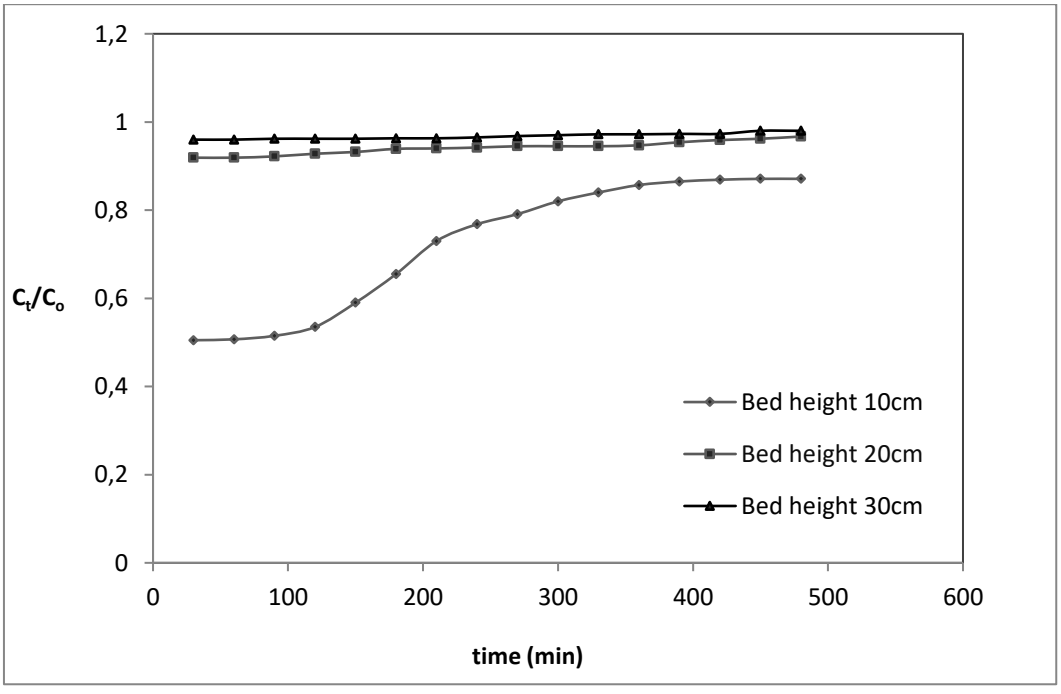

Fig. 3. Adsorption MY on NaOH-activated carbon at various bed heights

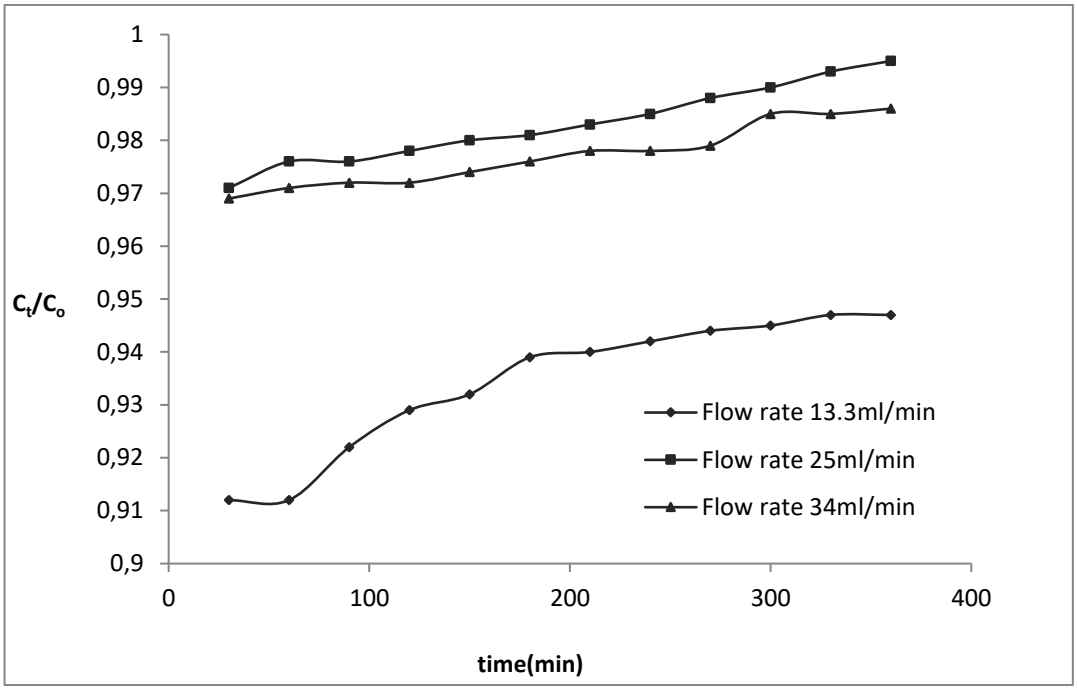

Fig. 4. Adsorption of MY on NaOH-activated carbon at various flow rates

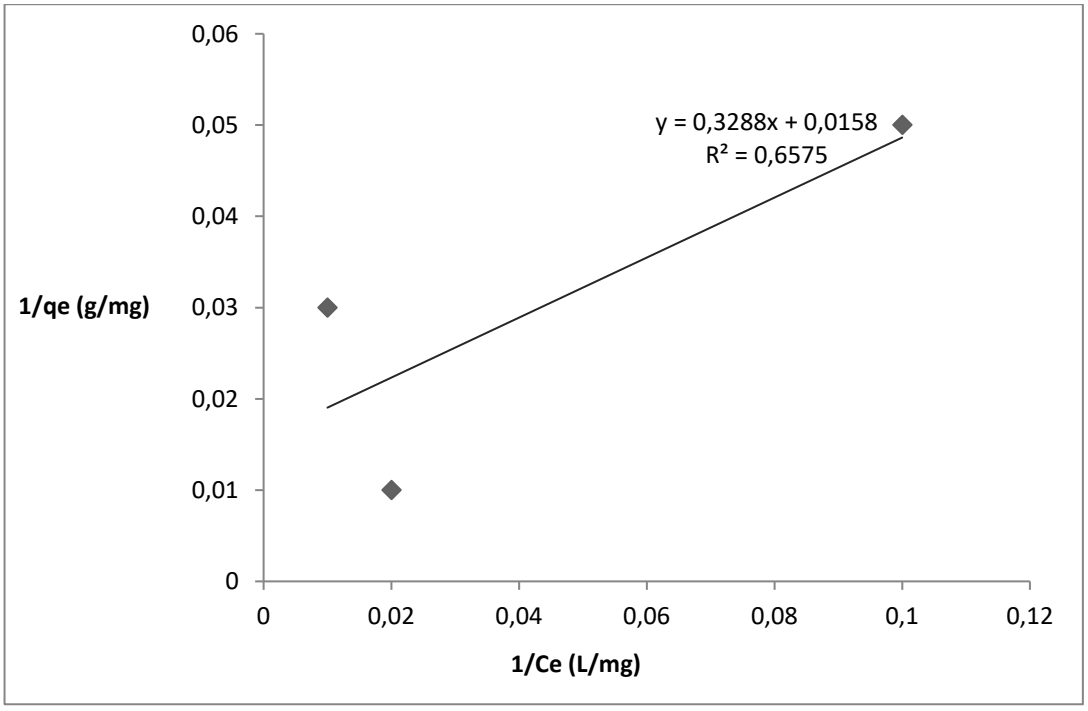

Fig. 5. Langmuir Type 2 isotherm model plot for adsorption of MY on NaOH-activated carbon

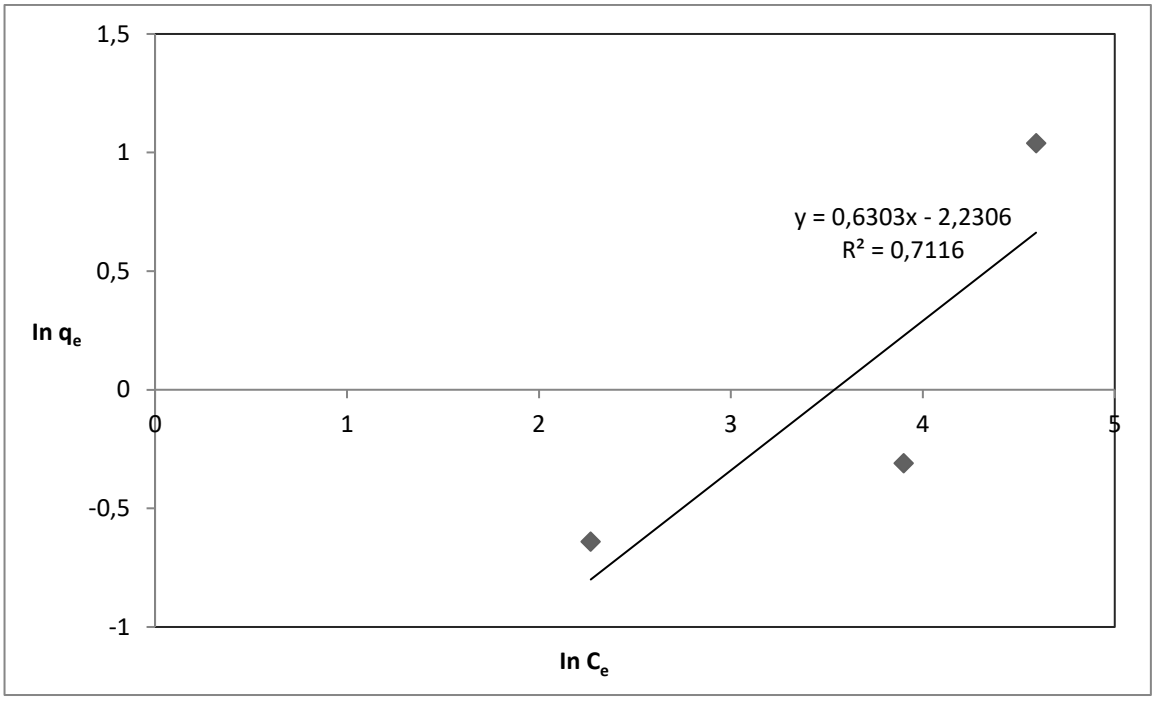

Fig. 6. Freundlich isotherm model plot for adsorption of MY on NaOH-activated carbon

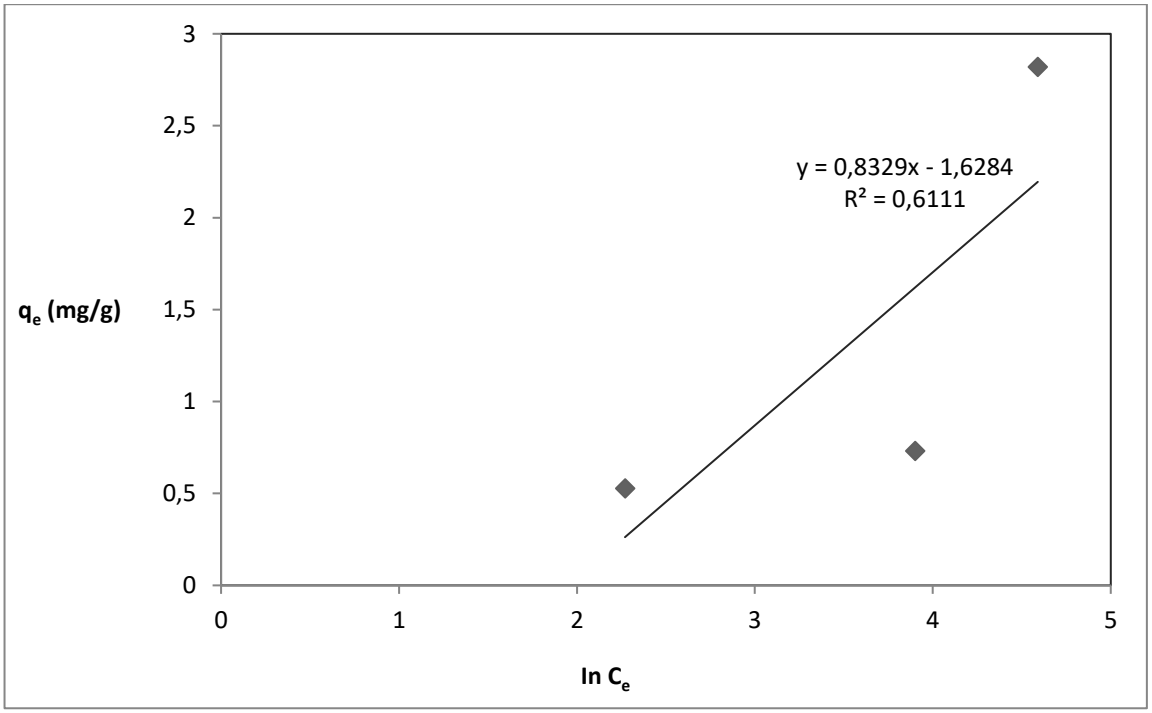

Fig. 7. Temkin isotherm model plot for adsorption of MY on NaOH-activated carbon

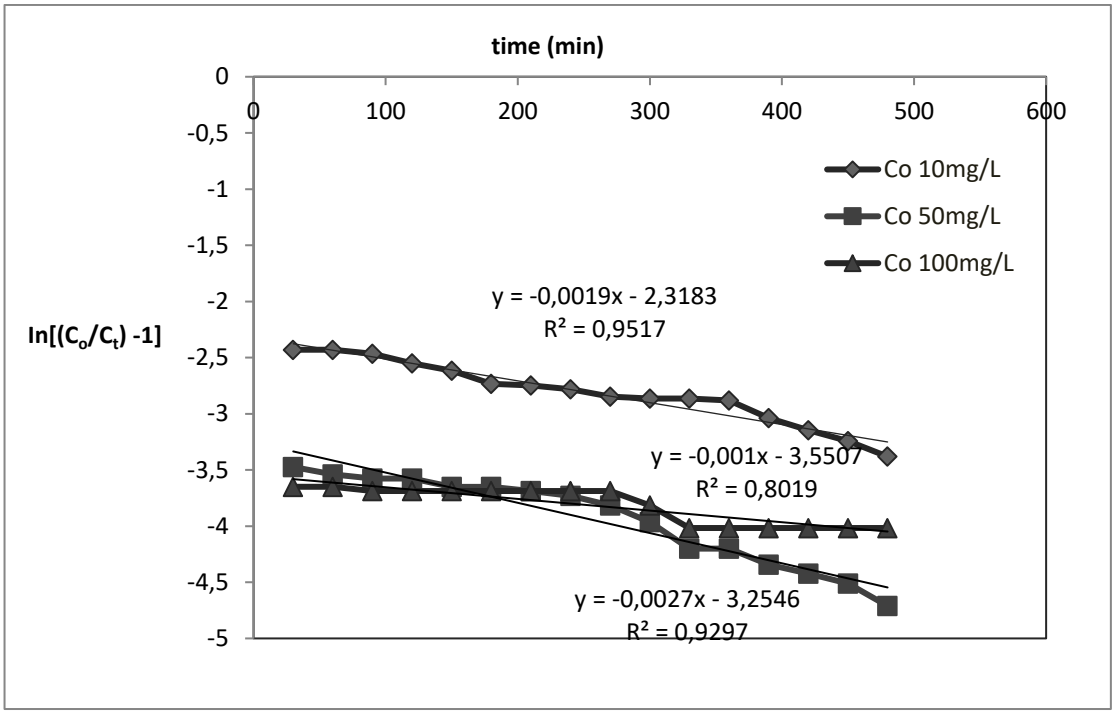

Fig. 8. Thomas plot model for the adsorption of MY on NaOH-activated carbon at various C_o

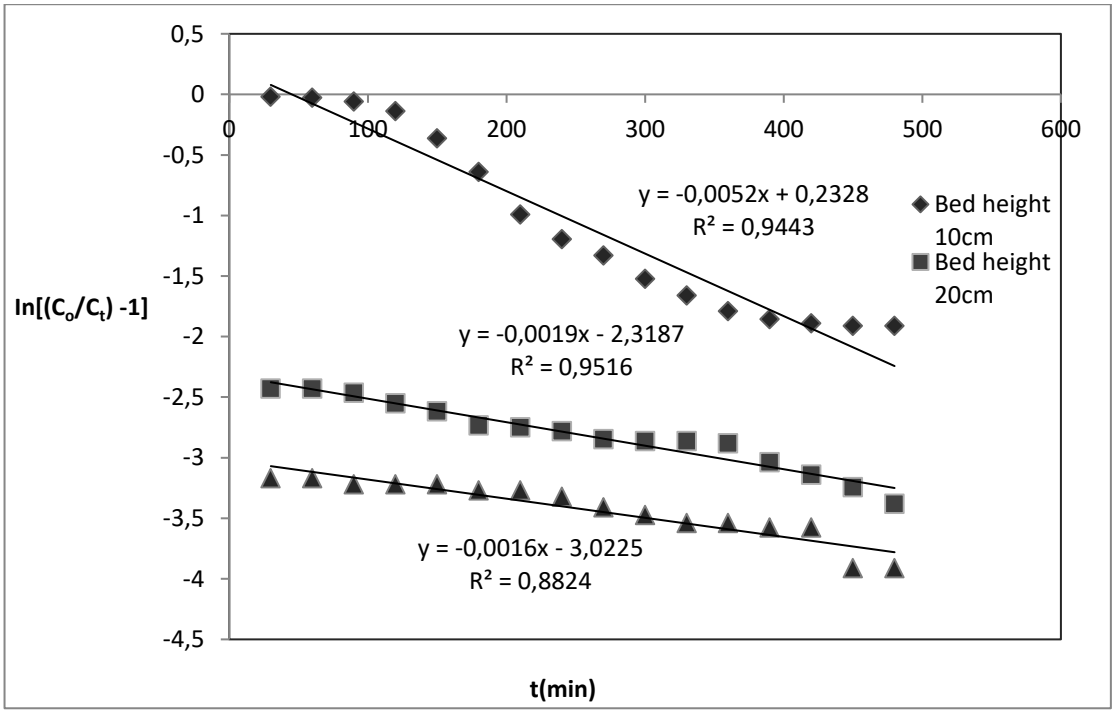

Fig. 9. Thomas model plot for the adsorption of MY on NaOH-activated carbon at various bed heights

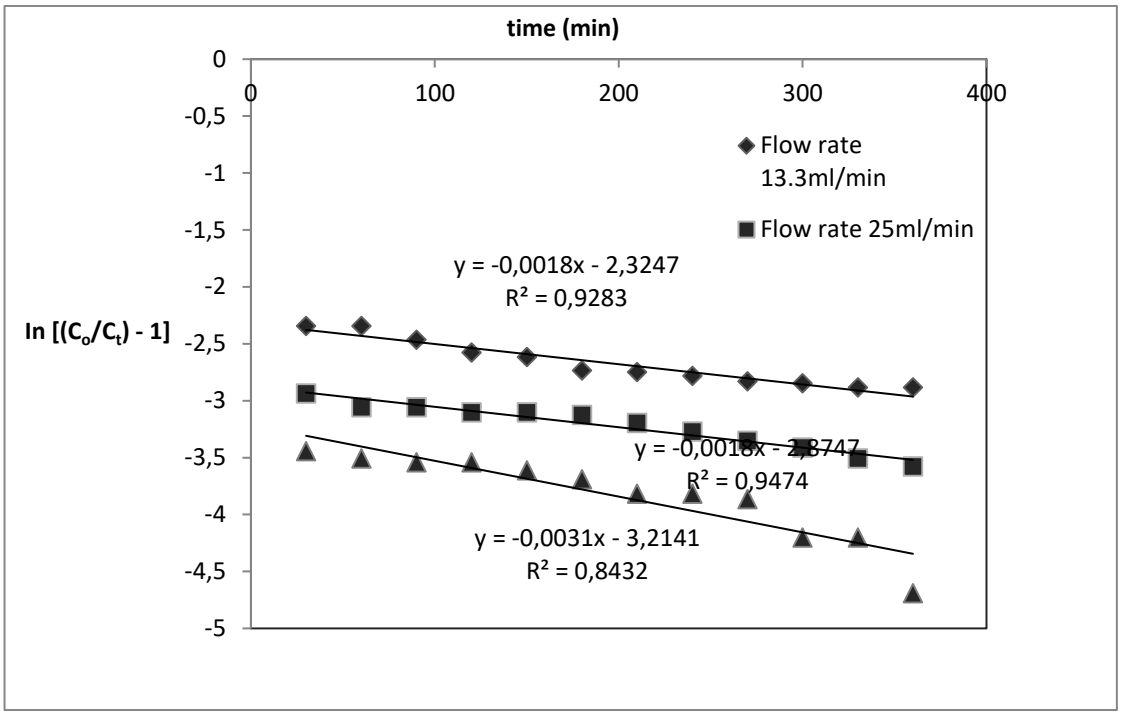

Fig. 10. Thomas model plot for the adsorption of MY on NaOH-activated carbon from at various flow rates

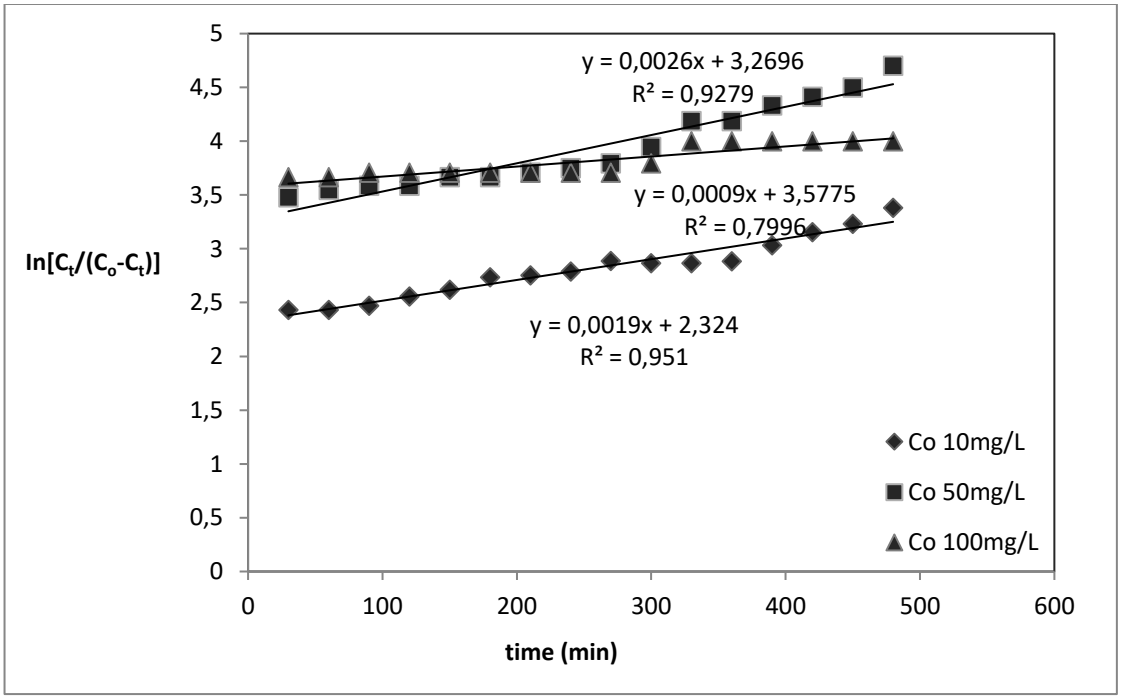

Fig. 11. Yoon-Nelson model plot for the adsorption of MY on NaOH-activated carbon at various C_o

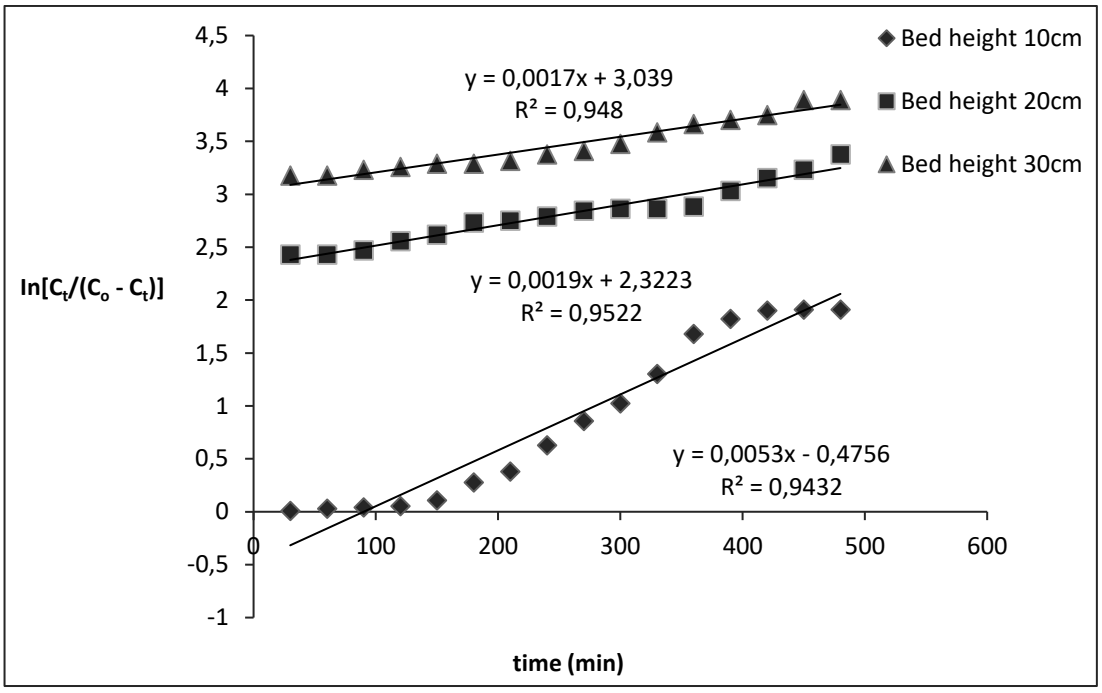

Fig. 12. Yoon-Nelson model plot for the adsorption of MY on NaOH-activated carbon at various bed heights.

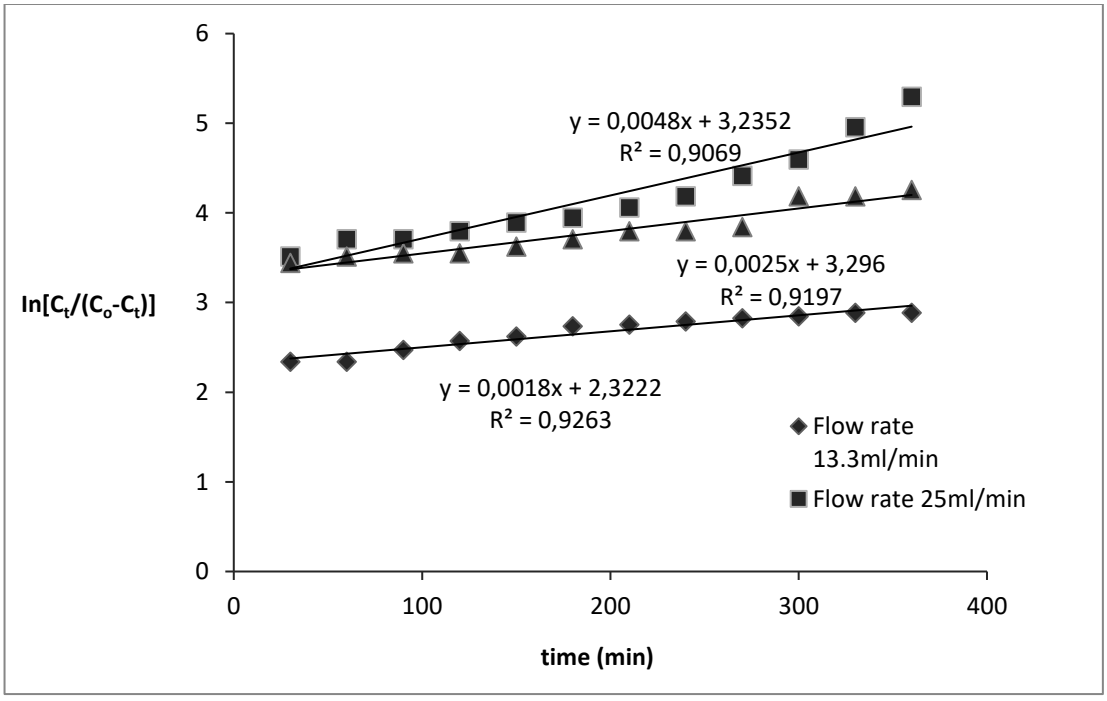

Fig. 13. Yoon-Nelson model plot for the adsorption of MY on NaOH-activated carbon at various flow rates.

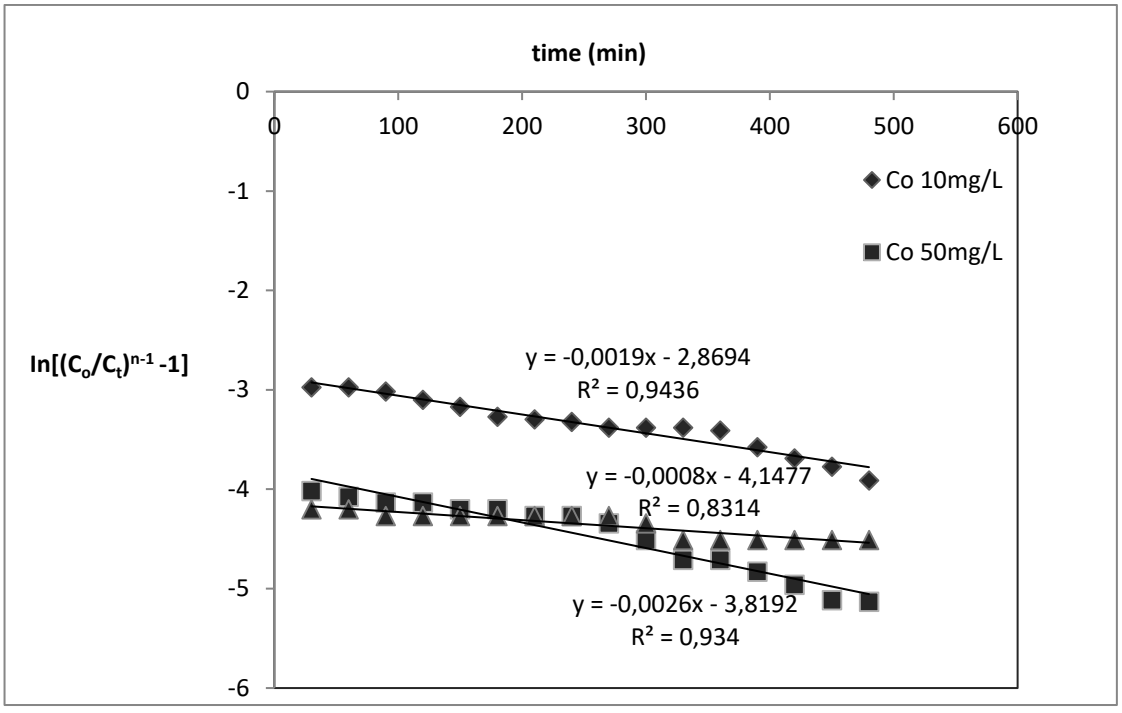

Fig. 14. Clark kinetic model plots for adsorption of MY on NaOH-activated carbon at various C_o

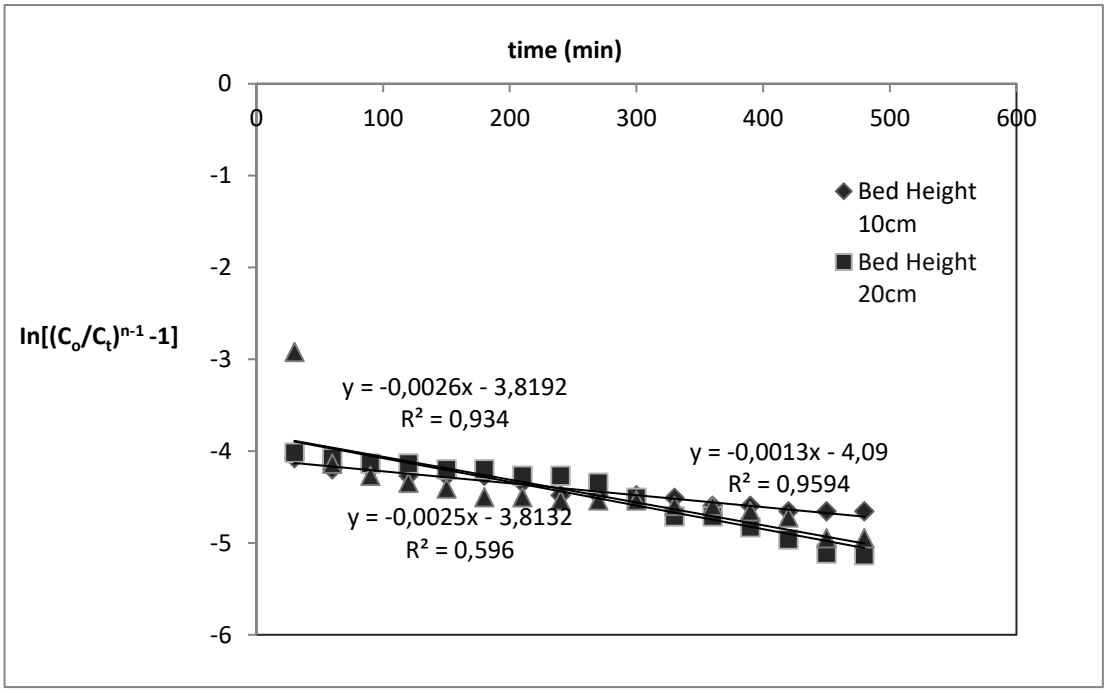

Fig. 15. Clark kinetic model plots for adsorption of MY on NaOH-activated carbon at various bed heights

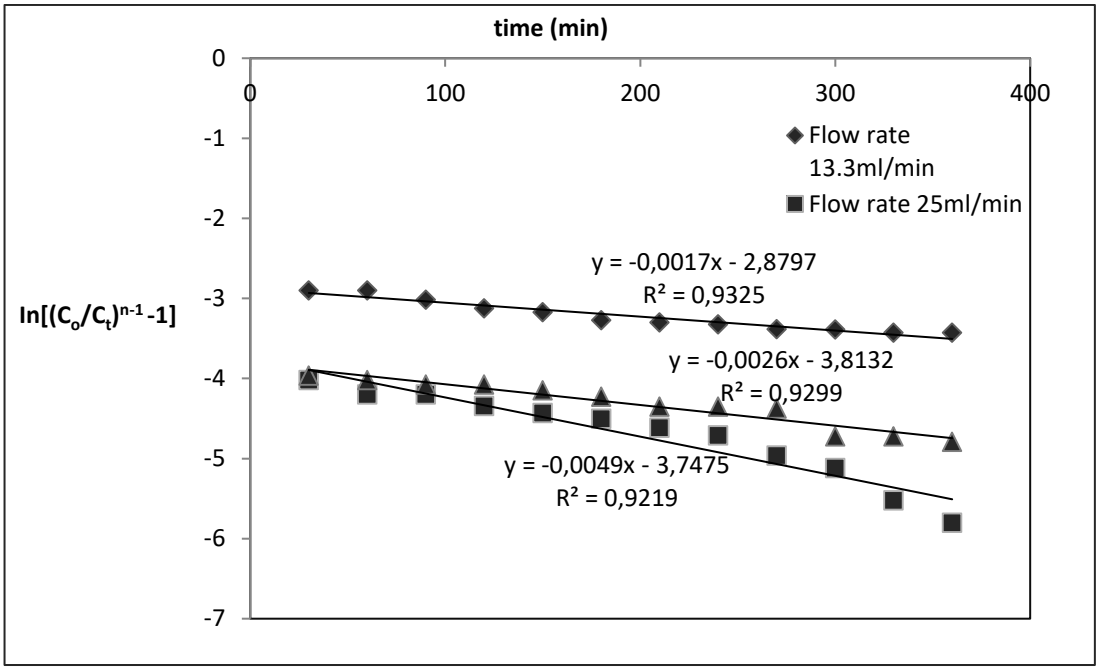

Fig. 16. Clark kinetic model plots for adsorption of MY on NaOH-activated carbon at various flow rates